euspen's 25th International Conference & Exhibition, Zaragoza, ES, June 2025
www.euspen.eu

Additively manufactured porous restrictor for aerostatic bearing

Onni Leutonen[1], Roy Björkstrand[1], Mikael Miettinen[1], Mika Salmi[1], Raine Viitala[1]

[1]*Aalto University*

onni.leutonen@aalto.fi

Abstract
Porous aerostatic bearings commonly consist of a porous restrictor joined to a bearing body with adhesive. Porous graphite is a typical material used for the porous restrictors. Material properties of graphite may vary significantly between manufacturing batches influencing the performance of the bearing. Additive manufacturing methods for porous metal for aerostatic bearings have been suggested as a potential method for manufacturing restrictors with defined permeability. The critical parameter values have not been disclosed, and the repeatability of the manufacturing process has not been studied. This study investigates the suitable parameters for the manufacturing of stainless steel porous aerostatic bearing restrictors with laser-based powder bed fusion of metals (PBF-LB/M) additive manufacturing method. The controlled parameter was the distance between laser scan lines. The effect of hatch spacing parameter, turning, and grinding on the permeability of the porous material was experimentally investigated. The results verify that the manufacturing method is suitable for controlling the permeability of the restrictor to a sufficient level. The results enable the selection of more suitable parameters for manufacturing porous aerostatic bearing restrictors.

Additive manufacturing, gas bearing, externally pressurized bearing, porous metal, laser-based powder bed fusion of metals

1. Introduction

Aerostatic bearings are commonly utilized in precision engineering due to the negligible friction and absence of the stick-slip effect. A high-pressure gas film is formed between the bearing and the opposing surface by applying pressure from an external source [1]. Air consumption is regulated by an inlet or outlet restrictor [2]. Bearing restrictor is typically nozzle, groove, or porous material [1, 2]. Porous material aerostatic bearings distribute the pressure evenly achieving increased load capacity and stiffness compared to other aerostatic bearing types [1, 2].

Porous aerostatic bearing restrictors are typically sintered metal, ceramic or porous graphite [3]. Graphite is commonly used due to the crash resistance of the material [3]. Porous graphite restrictor permeability varies affecting the bearing performance [3, 4, 5]. To achieve consistent bearing performance the permeability of porous graphite restrictors can be decreased via lacquer impregnation [6]. Typical permeability for the restrictors for optimal static and dynamic characteristics is from 10^{-14} m^2 to 10^{-16} m^2 [7].

Additive manufacturing of porous metal restrictors with laser-based powder bed fusion of metals (PBF-LB/M) has been presented in the literature [8, 9]. Porosity is a common defect in parts manufactured with PBF-LB/M. Additive manufacturing enables the permeability of the restrictor to be varied with manufacturing parameters including hatch spacing [8] and laser power [9]. These parameters affect the volumetric energy density (VED), which is the amount of energy brought to a volume of material. Decreasing the VED leads to incomplete melting of the powder and porosity in the final part. The mean permeability can be varied but also the permeability within the same restrictor can be varied locally [8, 9].

Additionally, additive manufacturing enables the whole bearing to be manufactured as a single component, as selected sections can be made porous or solid. This removes the need for a commonly used adhesive bond between the restrictor and the body, which improves the temperature tolerance of the bearing. PBF-LB/M enables the bearing to be manufactured from a variety of materials, therefore improving the material compatibility and chemical resistance.

One of the problems with ductile material is the smearing which makes the permeability control difficult [7]. The restrictor surface flatness requirement may necessitate the machining of the porous surface.

This study aims to validate the feasibility of manufacturing porous metal restrictor for aerostatic bearings with PBF-LB/M and discover suitable manufacturing parameters. In the present study, the effects of hatch spacing parameter, restrictor surface turning and grinding on the permeability of the porous restrictor were experimentally investigated.

2. Methods

2.1. Sample manufacturing

A batch of 12 samples with varying hatch spacing was manufactured with EOS M 290 from PH1 stainless steel powder with a layer height of 40 µm, laser spot diameter of 80 µm and scan speed of 1083 mm/s. The manufactured samples were disks with diameter of 37 mm and height of 5 mm. 0.5 mm of the outer edge was printed solid. The middle section was printed with an aligned meander pattern with 90˚ rotation and varying hatch spacing. Samples were printed without upskin or downskin to expose the porous section. A support structure was used between the build plate and sample to add extra material to be cut when separating the sample from the build plate.

When the laser spot diameter is smaller than hatch spacing, the VED can be calculated with Equation 1, where P is the laser power, v is the scan speed, d_{lb} is the laser spot diameter, and t is the layer height [10]. This equation only considers the volume scanned by the laser spot and omits the volume between scan lines. To estimate the average VED in the print area, the VED value is multiplied by the ratio between the laser spot diameter d_{lb} and the hatch spacing d_h. The average VED is therefore calculated with Equation 2.

$$E_V = \frac{P}{v d_{lb} t} \quad (1)$$

$$E_{VA} = \frac{P}{v d_{lb} t} \frac{d_{lb}}{d_h} = \frac{P}{v d_h t} \quad (2)$$

This average VED equation is the same as the VED equation when the laser spot size is larger than the hatch spacing [10].

The hatch spacing parameters and the corresponding average VED values are presented in Table 1. The used sample average VED and the theoretical average VED as a function of hatch spacing is presented in Figure 1 with VED reference values used by Sadahiro et al. [9]. The laser power parameter was adjusted in the study, and therefore, the local VED and porosity are approximately constant [9]. In this study, the hatch spacing parameter was adjusted, therefore the surface has mostly solid sections at the scan lines, where VED is approximated as E_V, and more porous sections between the scan lines where the VED is approximated as zero.

Table 1. Hatch spacing parameter values.

Sample	Hatch spacing (µm)	VED (J/mm³)
1	110	47.22
2	120	43.28
3	130	39.95
4	140	37.10
5	150	34.63
6	160	32.46
7	170	30.55
8	180	28.86
9	190	27.34
10	200	25.97
11	210	24.73
12	220	23.61

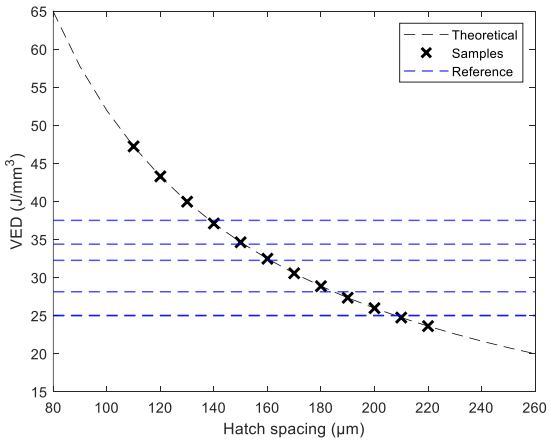

Figure 1. Sample average volumetric energy densities and reference values by Sadahiro et al. [9]. Hatch spacing was not available for reference values.

The samples were cut with wire electrical discharge machining (EDM). The sample restrictor disks were bonded to metal bodies with epoxy adhesive. Adhesive was used to enable pressure to be supplied without leakage past the restrictor. The bodies have integrated air supply grooves to distribute the pressurised air behind the porous restrictor. The sample geometry is presented in Figure 2. In addition to wire EDM, the samples were turned and ground. The short circuit airflow of the samples was measured after each step.

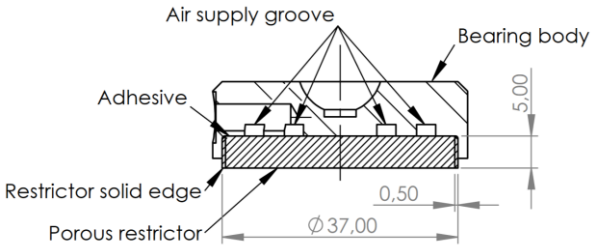

Figure 2. Sample geometry.

2.2. Short circuit flow and permeability

The short circuit flow rates were measured to determine the sample permeability. Short circuit flow rate is dependent on the size of the bearing, but sample permeability enables more general analysis and comparison.

The short circuit flow rates of the samples were measured by applying a 0.6 MPa supply pressure to the bearing with no opposing surface and measuring the flow rate after the flow had stabilised. Due to the vast flow rate range, sensors with measurement ranges of up to 2 L/min, 25 L/min, 50 L/min and 200 L/min were used. The flow rate was measured from the pressurized air supply line before the tested sample. The minimum measurable flow rate was 0.02 L/min, and all sensors had ±2% full range accuracy.

The sample permeability κ can be calculated with Equation 3 where Q_{SC} is the short circuit flow rate, μ is the dynamic viscosity of air, h is the porous restrictor height, A is the surface area of the restrictor porous section, p_s is the supply pressure and p_a is the ambient pressure [6].

$$\kappa = \frac{2 Q_{SC} \mu h p_a}{A(p_s^2 - p_a^2)} \quad (3)$$

3. Results and discussion

The surfaces of the manufactured restrictor samples were imaged with an optical microscope after each processing step, wire EDM, turning and grinding. The short circuit flows of the samples were also measured at these steps. Exemplary images of the surfaces of representative samples are presented in Figures 3, 4 and 5.

The wire EDM cut surface of sample 8 with 180 µm hatch spacing is presented in **Figure *3*** where a distinct grid pattern of pores can be observed. The solid lines between the pores were measured with a microscope to be approximately 100 µm to 110 µm and the diameter of the pores were approximately 70 µm to 80 µm. The laser spot diameter was 80 µm and the distance between the scanned lines with 180 µm hatch spacing was 100 µm. The surfaces of the wire EDM cut samples were convex presumably due to the internal stress from the manufacturing process.

The turned surface of sample 8 is presented in Figure 4. The turning process obstructs most of the pores presumably due to the ductility of the material. This forms a thin restrictive layer.

The ground surface of the sample 8 is presented in Figure 5. Similar to the turned surface, most of the pores were obstructed, and the grinding process did not open the pores. The surfaces of the ground samples were concave presumably due to the force applied by the fixture while grinding.

The short circuit flows of the wire EDM cut, turned, and ground samples are presented in Figure 6. The effect of the turning process obstructing the pores can be observed as a significant decrease in short circuit flow. The grinding process decreases the short circuit flow slightly further. The samples with zero

measured short circuit flow are omitted from permeability analysis.

Similar observations can be made from the permeability values presented in Figure 7. An increased hatch spacing increases the permeability significantly and the machining of the surface decreases the permeability.

The infill pattern with varied hatch spacing enables the formation of a grid of pores in the material, and therefore, the permeability of the restrictor can be adjusted with the hatch spacing parameter. Due to the warping of the restrictor after it was wire EDM cut from the build plate, the restrictor would not be suitable as an aerostatic bearing restrictor without further processing.

Turning and grinding of the surface decreases the permeability as a low permeability surface restrictor is formed due to the smearing of the ductile material. Most of the turned and ground samples with measurable flow have permeability within the optimal range from 10^{-14} m^2 to 10^{-16} m^2. Different methods of processing the restrictor surface should be studied to reach a suitable surface profile and restrictor permeability.

The warping of the restrictor could be mitigated by decreasing the internal stress with heat treatment before EDM cutting from the build plate. Heat treatment could also increase the hardness of the surface, decreasing the smearing during machining of the surface.

The repeatability of the manufacturing and surface processing should be studied as the sample size in this study was only one sample per parameter value.

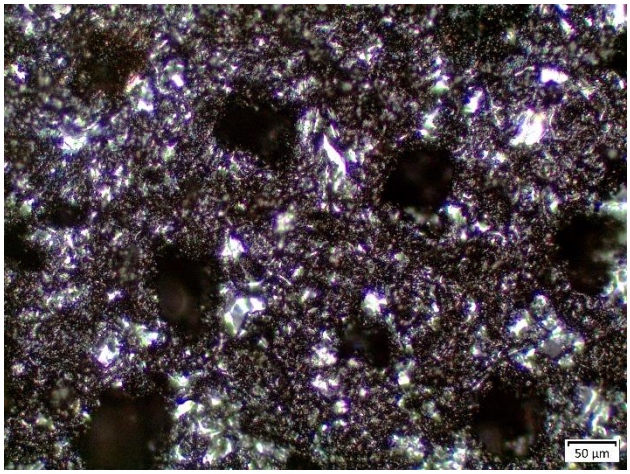

Figure 3. EDM cut surface of sample 8 with 180 µm hatch spacing.

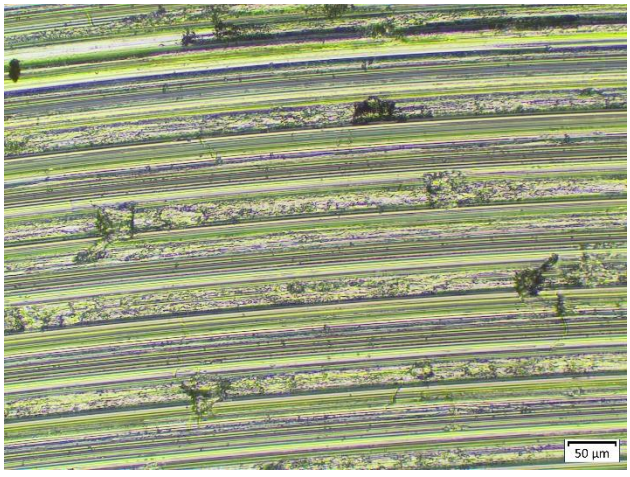

Figure 4. Turned surface of sample 8 with 180 µm hatch spacing.

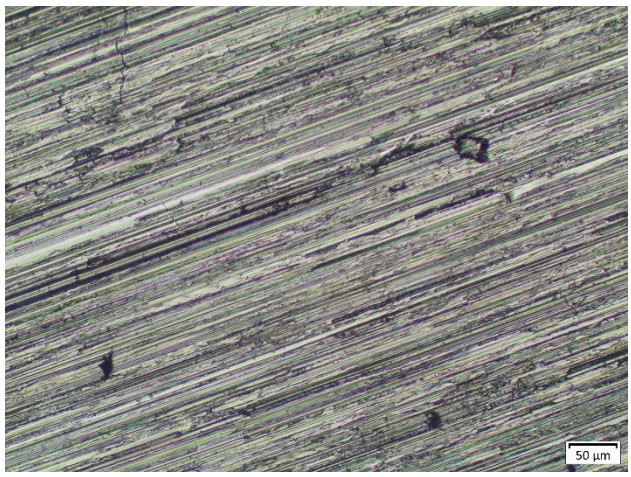

Figure 5. Ground surface of sample 8 with 180 µm hatch spacing.

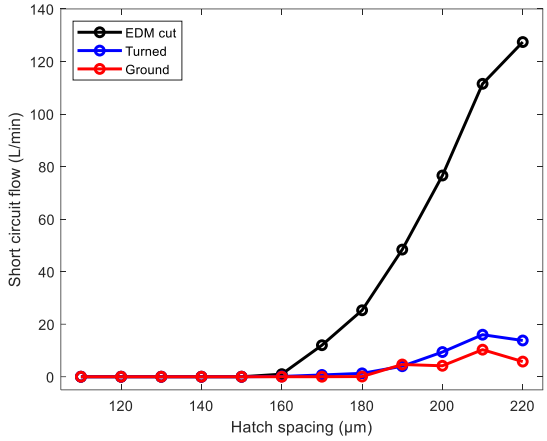

Figure 6. Sample short circuit flow rates at $p_s = 0.6\ MPa$.

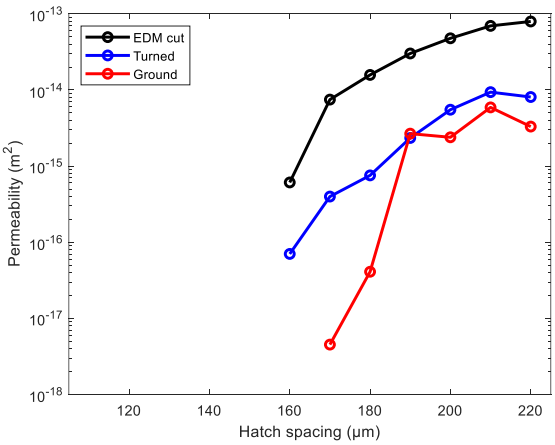

Figure 7. Sample permeability. Samples with zero flow omitted due to the logarithmic scale of the vertical axis.

4. Conclusions

The results of this study verify that porous metal restrictors for aerostatic bearings can be manufactured with PBF-LB/M, and the permeability can be controlled with the manufacturing parameters. The permeability increases with the increase in the varied hatch spacing parameter. The wire EDM cut surface shows a distinct grid pattern of pores. The permeability of the restrictor can be decreased with machining, as the cutting forces smear the ductile material, and a thin restrictive layer is formed.

Typical aerostatic bearing restrictor permeabilities were reached.

The repeatability of the manufacturing method should be studied in future work, as in this study, only one sample per parameter value was manufactured and investigated. Furthermore, heat treatment to reduce internal stress and warping of the part could be studied. Heat treatment could also increase the hardness and thus reduce the smearing of the restrictor. Additionally, the effect of machining parameters on the permeability could be studied.

5. Acknowledgements

The research was funded by Business Finland (Power Beyond, grant number 2534/31/2022).

Part of the research was performed at the Aalto Digital Design Laboratory of Aalto University.

References

[1] Slocum A H 1992 *Precision Machine Design* (Prentice Hall).

[2] Wardle F 2015 Aerostatic bearings *Ultra-Precision Bearings* (Elsevier) pp 227–306 doi: 10.1533/9780857092182.227

[3] Al-Bender F 2021 Porous bearings *Air Bearings - Theory, Design and Applications* (John Wiley & Sons) pp 403–24

[4] Miettinen M, Vainio V, Theska R and Viitala R 2024 On the static performance of aerostatic elements *Precision Engineering* **89** pp 1–10 doi: 10.1016/j.precisioneng.2024.05.017

[5] Vainio V, Miettinen M, Majuri J, Theska R and Viitala R 2023 Manufacturing and static performance of porous aerostatic bearings *Precision Engineering* **84** pp 177–90. doi: 10.1016/j.precisioneng.2023.06.014

[6] Rasnick W H, Arehart T A, Littleton D E and Steger P J 1974 Porous graphite air-bearing components as applied to machine tools *Society of manufacturing engineers* (Dearborn)

[7] Cappa S, Reynaerts D and Al-Bender F 2014 Reducing the radial error motion of an aerostatic journal bearing to a nanometre level: Theoretical modelling *Tribology Letters* **53** pp 27–41 doi: 10.1007/s11249-013-0241-8

[8] Schoar S, Elspaß A, Dohmen H J, Kleszczynski S and Benra F 2021 Design and fabrication of optimised aerostatic dry gas seals using advanced numerical models and next generation production technology, *Polytechnic & design* **9** no 3 pp 156–66 doi: 10.19279/TVZ.PD.2021-9-3-11

[9] Sadahiro R, Nakayama S, Kawada S, Miyatake M, Sasaki S and Yoshimoto S 2023 Development of aerostatic porous bearings manufactured using metal 3d printing technology *Proc. IMechE, Part J: Journal of Engineering Tribology* **237** pp 1306–15 doi: 10.1177/13506501211070090

[10] Agrawal A K, Meric de Bellefon G and Thoma D 2020 High-throughput experimentation for microstructural design in additively manufactured 316l stainless steel *Materials Science and Engineering: A* **793** 139841 doi: 10.1016/j.msea.2020.139841